Isoform-specific O-glycosylation dictates Ebola virus infectivity

Ieva Bagdonaite[1,*], Samir Abdurahman[2], Mattia Mirandola[3], Yoshiki Narimatsu[1], Sergey Y. Vakhrushev[1], Cristiano Salata[3], Ali Mirazimi[2,4,5,*], and Hans H. Wandall[1,*]

[1] Copenhagen Center for Glycomics, Department of Cellular and Molecular Medicine, University of Copenhagen, Copenhagen 2200, Denmark

[2] Public Health Agency of Sweden, Solna 17165, Sweden

[3] Department of Molecular Medicine, University of Padua, Padua 35121, Italy

[4] Department of Laboratory Medicine (LABMED), Karolinska Institute, Stockholm 17177, Sweden

[5] National Veterinary Institute, Uppsala 75189, Sweden

*Correspondence: hhw@sund.ku.dk (H.H.W.), ieva@sund.ku.dk (I.B.) and ali.mirazimi@folkhalsomyndigheten.se (A.M.)

Abstract

Ebola virus glycoprotein is one of the most heavily O-glycosylated viral envelope glycoproteins. The glycoprotein possesses a large mucin-like domain responsible for the cytopathic effect on infected cells, yet its structure or potential role in early entry events is poorly defined. To understand the importance of elongated O-glycans and the individual O-glycosylation sites for viral infectivity, we performed a comprehensive characterization of site-specific glycosylation governed by the three key GalNAc-transferases, GalNAc-T1, -T2, and -T3, initiating O-glycan biosynthesis. Using TMT isobaric labelling we performed quantitative differential O-glycoproteomics on proteins produced in wild type HEK293 cells and cell lines ablated for each of the three GalNAc-Ts, as well as compared it to patterns on wild type virus-like particles. In total we found 38 and 41 O-glycosites on virus like particle-derived and recombinant GP, respectively, with well correlated sites and site-specific structures. Examination of the isoform-specific glycosylation demonstrate selective initiation of a subset of O-glycosites by each enzyme, with GalNAc-T1 having the largest contribution. We next demonstrate that O-linked glycan truncation and perturbed initiation retarded the production of viral particles and decreased infectivity of progeny virus. This work represents a comprehensive site-specific analysis of EBOV GP and sheds light on differential regulation of EBOV GP glycosylation initiated by host GalNAc-Ts. Together with the effect on viral propagation it opens prospective avenues for tailored intervention approaches and means for modulating immunogen O-glycan density.

Introduction

Ebola virus (EBOV) is a deadly enveloped filovirus that causes recurrent outbreaks of deadly hemorrhagic fever primarily in Africa. The zoonotic nature of the virus poses a formidable threat in densely populated regions. The most recent outbreaks in West Africa (EBOV Makona) and The Democratic Republic of Congo in 2014 and 2018-2020, respectively, were the most widespread so far and claimed numerous lives. This also led to a search of means to tame the disease and resulted in development of therapeutic antibody cocktails and vaccines [1-5]. However, affordable and widely available treatments are still lacking.

The EBOV glycoprotein (GP) is the only viral protein on the surface of the virion and is critical for attachment to host cells and catalysis of membrane fusion. The GP is a transcriptionally edited transmembrane glycoprotein which is proteolytically processed by a furin-like host protease to yield covalently linked GP1 and GP2 that form trimers of heterodimers (Fig. 1A, 1B) [6]. GP1 mediates cellular attachment in a macropinocytosis-dependent manner by engaging TIM-1, DC-SIGN and other C-type lectins, whereas GP2 executes fusion upon interaction with NPC intracellular cholesterol transporter 1 (NPC1) that thereby acts as an endosomal entry receptor [7-11]. A substantial portion of GP1 is comprised of heavily glycosylated glycan cap domain (GCD) and mucin-like domain (MLD), which collectively occlude the NPC1 binding site, and therefore need to be cleaved off by cathepsins L and B for proper infectivity (Fig. 1A, 1B). Furthermore, an additional priming event is needed in the endosomal compartment to ensure interaction with NPC1 and fusion [12-15].

Glycosylation of viral envelope glycoproteins rely on the glycosylation machinery of the host [16]. The most predominant types of glycans in humans include N-linked glycans and mucin-type O-linked glycans [17]. N-linked glycans modify asparagine residues within N-X-S/T ($X \neq P$) sequons and have extensively been characterized on various viral envelope glycoproteins and are easy to predict [18-21]. O-glycan initiation is regulated by the competing action of 20 isoforms of polypeptide GalNAc-transferases in humans [22]. While there is some knowledge on isoform-specific protein substrates, their non-redundant roles in glycosylating viral envelope proteins have not been addressed [23-26]. Up to eight core structures have been described for O-GalNAc glycans, though core 1 and core 2 are the most ubiquitously encountered (Fig. 1C) [27, 28].

GP1 contains 17 N-glycosylation sequons in both the GCD and the MLD; 12 of them are predicted to be utilized (Fig. 1A). A few specific N-glycosites affecting EBOV conformational stability or immunogenicity have been identified and shown to provide steric shielding of host cell ligands for immune effector cells [29, 30]. The MLD is also predicted to be heavily glycosylated, though no specific sites have been identified, and the studies on O-glycosylation have been limited to deletion of MLD [30-32]. The extent and role of O-glycosylation in EBOV biology is thus still obscure. Moreover, the structure of the MLD, comprising at least half of GP's mass [33], is poorly defined, as the region is usually omitted from crystallographic studies (Fig. 1B) [34].

Mutational studies have identified the MLD being responsible for EBOV-induced cytotoxicity and vascular permeability [35]. MLD has also been hypothesized to protect from antibody neutralization, as removal of glycan cap during cathepsin processing would expose immunodominant residues important for receptor binding or cell fusion, and better neutralization of *in vitro* pre-processed pseudotyped particles by convalescent plasma was achieved [36]. Given the involvement of the MLD in various stages of viral life cycle and immune recognition, it is important to better understand its structural features, including the predominant glycan structures, their sites, and the regulation of glycan density by GalNAc-transferases.
Here, we used tandem mass spectrometry to map O-glycosylation sites on Makona strain EBOV GP and determine the individual contribution of GalNAc-T1, -T2, and -T3 to O-glycan initiation. Furthermore, we investigated the role of O-linked glycan initiation and elongation for EBOV propagation using genetically engineered cell lines and discovered requirement of all five investigated gene products for proper infectivity of progeny virus.

Results

EBOV exhibits diminished propagation in O-glycosylation mutant cell lines

In order to address the function of O-glycans in EBOV biology, we infected HEK293 cells lacking O-linked glycan elongation (*C1GALT1C1* KO), or deficient in individual isoforms of predominant initiating enzymes (*GALNT1* KO, *GALNT2* KO or *GALNT3* KO) (Fig. 1D). Intracellular viral replication was diminished in all mutant cell lines compared to wild type on both Day 1 and Day 6 post infection (Fig. 1E). The trend was also reflected in amounts of extracellular viral RNA on Day 6 post infection, with deletion of individual *GALNT* genes having a larger effect compared to elimination of O-glycan elongation (Fig. 1F). We then measured viral titers in cell culture supernatants to evaluate the infectivity of extracellular virions. On Day 1 post-infection, viral titers in supernatants of all four knock out cell lines were slightly lower but still comparable to wild type (Fig. 1G). In contrast, a substantial reduction in viral titers was observed in all four knock out cell lines on Day 6 post-infection (Fig. 1G). The combined data suggests the importance of both O-glycan initiation by the individual GalNAc-T isoforms and O-glycan elongation for sustained viral propagation.

EBOV GP is expressed on the surface of glycoengineered cells

Reduced titers of extracellular virions could result from a number of different issues, including but not limited to viral envelope GP expression, trafficking, and function. To assess EBOV GP expression in glycogene knock out cell lines (*C1GALT1C1* KO, *GALNT1* KO, *GALNT2* KO and *GALNT3* KO (Supplementary Fig. 1)) we investigated both native virus-infected cells (Fig. 2A, 2B), and those transfected with a recombinant full lenth GP (Fig. 2C). Immunofluorescence staining of infected wild type cells at low MOI revealed smaller and larger clusters of infected cells with predominant surface expression of GP (Fig. 2A, 2B). Aside from *GALNT2* KO cells often exhibiting very small lesions (Fig. 2A, 2B *GALNT2* KO lower images), all KO cell lines appeared competent for GP surface expression. To confirm GP surface expression in non-permeabilized cells, we expressed full length EBOV GP in the suite of glycoengineered cell lines and co-stained them with surface marker E-cadherin (Fig. 2C). In agreement with infected cell data, recombinant GP was detected on the surface of all five cell lines. This suggests that alterations in O-glycosylation do not impair glycoprotein trafficking. Furthermore, it allowed us to use the glycoengineered cell lines for recombinant GP production for the analysis of how the individual GalNAc-T isoforms define the O-glycosylation pattern of GP.

Different GalNAc-T isoforms glycosylate distinct sites within the MLD

Cumulative reduction of viral titers over time suggested that modulation of O-glycan length and density may have an effect on MLD stability or function. We therefore wanted to generate a more comprehensive knowledge of the O-glycans that decorate the MLD and next mapped specific O-glycosites, their predominant structures, and site-selective initiation by GalNAc-T isoforms. In order to identify O-linked glycosylation sites on EBOV GP, we analyzed EBOV virus-like particles (VLPs) presenting the GP on native-like rod-shaped particles generated by co-expression with VP40 protein, and representing the mature glycoprotein (Fig. 3A). To determine the individual contributions of GalNAc-T1, -T2, and T3, we expressed the full length His-tagged EBOV GP in WT and the different *GALNT* KO cell lines, purified and digested the protein, and labelled the resulting peptides with TMT isobaric mass tags allowing for relative quantification of (glyco)peptides in the different samples (Fig. 3B) [37, 38]. In both approaches, we performed sequential lectin weak affinity chromatography (LWAC) of desialylated tryptic digests to enrich for abundant core 1 O-glycan structures (T, Galβ1-3GalNAcα1-O-Ser/Thr) and their biosynthetic intermediates (Tn,

GalNAcα1-O-Ser/Thr) using peanut agglutinin (PNA) and *Vicia villosa* lectin (VVA), respectively. We identified 47 O-glycosites, 45 of which unambiguous, majority of which located to MLD and glycan cap regions and were in good agreement between VLPs and purified GP, with 32 O-glycosites in common (Fig. 4A, Table 1, Supplementary Dataset 1). PNA LWAC allowed for enrichment of not only core 1, but also core 2 structures, which were abundantly found at the majority of glycosites. Notably, core 2 structures often co-existed on adjacent amino acids, such as Thr326 and Ser327, Ser347 and Ser348, or Thr424 and Thr425. In contrast, we found a few GP stretches, where no elongation was taking place due to dense O-glycosylation, with up to seven glycosites identified on the same peptide (366-380), predominantly as single GalNAc structures. This signifies local structural differences in glycosyltransferase accessibility within different subregions of the MLD. Glycosites and site-specific structures identified on recombinant EBOV GP was in good agreement with those identified on VLPs, representing mature glycoproteins (Fig. 4A, Table 1). While many of the glycosites were identified on multi-glycosylated peptides, some of those sites were also covered by peptides only carrying a single O-glycan, possibly informing on the order of glycan addition. By quantifying the relative abundances of singly glycosylated peptides, we could evaluate the individual contributions of GalNAc-T1, -T2, and -T3 to specific sites (Fig. 3B, 3C, 4B). Non-redundant regulated glycosites could be identified for each isoform (Fig. 4A, 4B, Table 1) demonstrating that all three GalNAc-Ts contributed to complete glycosylation of EBOV GP. In addition, there were a few glycosites with contribution from several GalNAc-Ts, and we could also identify non-regulated sites, suggesting either preference by a different isoform, or non-selective glycosylation (Fig. 4B). GalNAc-T1 had by far the largest contribution, with selective regulation of at least seven O-glycosites, whereas GalNAc-T2 and GalNAc-T3 were responsible for one glycosite each (Fig. 3C, 4A). Moreover, knock out of GalNAc-T1 had a global effect on EBOV GP glycosylation and resulted in massive changes of both downregulated and upregulated glycopeptides (Fig. 3C), suggesting GalNAc-T1 is a major regulator of EBOV GP glycosylation, supported by a notable molecular mass shift of the protein (Supplementary Fig. 2). Interestingly, a big proportion of GalNAc-T1 regulated sites resided in close vicinity to N-glycosites, and most were found on de-amidated peptides, which likely were N-glycosylated before PNGase F treatment. Importantly, these glycosites were unambiguously localized to respective serines and threonines and often

harbored complex core 2 structures, excluding the possibility of artefactual GlcNAc “stumps” at N-glycosites.

O-glycosylation of host cells modulates entry of pseudotyped EBOV

To investigate the effect of O-glycosylation on EBOV GP function, we performed two sets of experiments with EBOV GP pseudotyped vesicular stomatitis virus (VSV). To address GP-mediated entry to cells lacking O-glycan elongation or isoform-specific initiation, we titrated wild type EBOV GP-VSV on the panel of glycoengineered cells and quantified the luciferase reporter expression upon entry. This revealed diminished entry to all mutant cell lines, suggesting host cell O-glycosylation may contribute to delayed propagation and decreased infectivity of live EBOV (Fig. 5A).

To address the functionality of pseudoparticles produced in the different knock out cell lines, the cells were transfected with EBOV GP encoding plasmid followed by infection with VSVΔG and titration of generated stocks on Vero cells. Pseudoviruses generated in the mutant cell lines exhibited similar titers to those in the wild type, though slightly lower titers were observed for *GALNT1* KO- and *GALNT3* KO-generated pEBOV, whereas the titer was slightly higher for *C1GALT1C1* KO-produced pEBOV (Fig. 5B). This suggests EBOV GP with altered O-glycosylation patterns is functional when presented on VSV surface. To investigate particle morphology of infectious EBOV, we performed transmission electron microscopy of virions present in cell culture supernantants of infected HEK293 cells 24 hours post-infection. We could detect characteristic rod-shaped virions in supernatants of all HEK293 KO cell lines (Fig. 5C). Aside from predominantly shorter *GALNT1* KO virions, we could not detect any gross changes in particle morphology. This does not exclude potential issues with particle functionality and ultrastructural studies would be needed to investigate GP distribution.

Discussion

Glycosylation of viral glycoproteins plays diverse important roles in infectivity and immune shielding [16]. Studies on glycosylation of viral envelope proteins of highly pathogenic viruses are challenging due to several limitations, including difficulties and biosafety concerns in using the fully infectious viruses as test subjects. Furthermore, there are no good ways of eliminating

specific glycosylation sites without introducing large deletions or single amino acid mutations, which may alter the conformation of proteins and provide misleading conclusions regarding the effect of glycosylation. Here, we used a panel of genetically engineered cells in the context of natural EBOV infection to evaluate the consequences of global changes in O-glycan structures or downregulation of O-glycans at specific sites by eliminating isoforms of enzymes responsible for O-glycan initiation. In addition, we mapped the individual O-glycosites on EBOV GP and identified those GalNAc-T regulated subsets by differential O-glycoproteomics, with GalNAc-T1 having the most pronounced role. In addition, we used infection with native Ebola virus and observed a striking reduction in viral titers, not only for *C1GALT1C1* KO and *GALNT1* KO, but also for *GALNT2* KO and *GALNT3* KO cell lines. This would suggest involvement of specific O-glycosylation sites in EBOV pathogenesis, which has been suggested by large deletions of MLD, and by effects on recombinant EBOV GP-induced cell rounding by O-glycan truncation and loss of GalNAc-T1 [39]. In addition, we have previously shown requirement of elongated O-linked glycans for efficient propagation of HSV-1, another heavily O-glycosylated virus [40].

Experiments with EBOV GP pseudotyped VSV particles suggested contribution of all three investigated GalNAc-Ts, as well as O-glycan elongation of the host cells, to entry of wild type pseudovirus. This could both be related to O-glycosylation of several C-type lectins and TIM-1, as well as overall changes in the glycocalyx organization due to multiple affected substrates not directly involved in pathogenesis. For instance, glycan-glycan interactions have been suggested important for early HIV-1 interactions with the host cell [41]. It is important to note that epithelial cells will present a limited repertoire of C-type lectins, and there might be other not yet defined proteins mediating early interactions. While O-glycosylation defects did not affect GP incorporation into pseudotyped virions or their entry via clathrin-mediated endocytosis, it does not exclude detrimental effects on live virions, exhibiting entirely different morphology and entering via macropinocytosis, and is yet to be addressed.

While it is well known EBOV GP is heavily O-glycosylated, specific glycosites or the extent of glycan density within the MLD have not been described in detail. To address this question, we performed O-glycoproteomic analysis of EBOV VLPs to estimate the total capacity of O-glycosylation in cells expressing a complete set of GalNAc transferases, and identified 38-specific O-glycosites primarily within the glycan cap and the MLD, and could confirm the majority of those sites on

recombinantly expressed GP with predominant core 1 and core 2 structures. By performing quantitative differential O-glycoproteomic analysis using *GALNT* KO cell lines, we found that GalNAc-T1 deficiency downregulated a large proportion of rather uniformly spaced O-glycosites and is expected to affect overall glycan density on the MLD, possibly also influencing its physical and immunological properties. GalNAc-T1 has previously been suggested to be responsible for MLD-induced cell rounding, and compound deletion of five specific Ser/Thr amino acids has achieved the same effect [39]. Four of those amino acids are homologous in our investigated strain, and we found three of them O-glycosylated. Of those, Thr334 was selectively glycosylated by GalNAc-T1, and may be responsible for the MLD-induced cytopathic effect via a yet undefined mechanism.

Regulation of O-glycan initiation by competing GalNAc-Ts is not completely understood, and while there is no consensus sequence for O-glycosylation in general, or the individual isoforms, there are slight differences in amino acid context preference by the individual catalytic domains [42, 43]. Furthermore, most GalNAc-Ts are capable of long-range follow-up due to positioning by the lectin domain recognizing distant already glycosylated sites, where varying linker length between the two domains determines the range [44-46]. The N-glycosite proximal GalNAc-T1 regulated sites may be a result of the lectin domain-positioned O-glycan initiation, given GalNAc-T1 prefers to follow up 8-10 residues N-terminally from existing O-glycosites [47, 48], which would fit well with e.g., regulated Thr334 and Ser348 each spaced by 10 amino acids from respective Ser344 and Thr448.

A few O-glycosites have been identified close to cathepsin L cleavage site, with Thr206 regulated by GalNAc-T1 and GalNAc-T2, absence of which may affect processing in the endocytic compartment. Similarly, a GalNAc-T3 regulated site (Thr494) was found close to furin cleavage site, and may play a role in protein maturation.

A number of immunodominant epitopes have been identified within the MLD and the glycan cap in animal studies, vaccine clinical trials and human survivors [49-51]. Interestingly, rather consistent antibody signatures have been identified in the less glycosylated GP2, whereas there is little correlation of antibody epitopes in GP1 containing mucin-like domain and glycan cap [52]. In non-human primates, vaccination approaches have generated the most immunodominant epitopes in the MLD, where class switched antibodies were also mapped to [51]. This may suggest

variable antibody signatures to immunogens bearing differential O-glycosylation patterns due to distinct GalNAc-transferase repertoires in production cell lines and natural hosts [18]. We found four O-glycosites (Ser475, Thr483, Thr485, and Thr494), two of them regulated, in the epitope region of 4G7 neutralizing antibody that is part of the ZMAb/ZMApp therapeutic antibody cocktails [49, 53]. Of those, Thr483 and Thr485 comprise epitopes for two other antibodies. In addition, Ser399, which we find glycosylated, is part of the epitope for 6D8 monoclonal antibody [53]. Understanding these signatures in relation to GalNAc-T repertoires and glycosite occupancy would be useful for understanding principles of neutralization and could help generate desirable immune responses by glycoengineering the immunogens.

Materials and methods

Cells, plasmids and viruses

The cell lines used were HEK293T/17 (HEK293T, ATCC® CRL-11268™), HEK293 WT (Sigma Cat. Nr. 85120602), HEK293 *GALNT1* KO [54], HEK293 *GALNT2* KO [54], HEK293 *GALNT3* KO [54], *C1GALT1C1* KO [55] bearing truncated O-glycans (SC), VERO (VERO-ccl81, ATCC® CCL-81™), and Vero-E6 cells (ATCC, CRL-1586™). All cell line were maintained in Dulbecco's Modified Eagle's Medium (Life Technologies Cat. Nr. 419660), supplemented with 10 % v/v of heat-inactivated Fetal Bovine Serum (FBS, Life Technologies Cat. Nr. 10500) and incubated at 37° C with 95 % humidity and 5% CO_2.

Zaire ebolavirus (ZEBOV isolate Ebola virus/H.sapiens-wt/SLE/2014/Makona-G3838) was propagated in Vero-E6 cells in T75 culture flasks. At day six post-infection, virus particles in cell culture supernatants were harvested and clarified from cell debris by centrifugation at 1,500 rpm for 10 min. The virus was then aliquoted in Eppendorf tubes, titrated in Vero-E6 cells cultured in 16-well chambered slides (Thermo Fisher Scientific) as described below and stored at -80 °C.

The plasmid expressing the Zaire ebolavirus (ZEBOV) Glycoprotein (isolate Ebola virus/H.sapiens-wt/SLE/2014/Makona-G3838), pcDNA3.1-ZEBOV-GP, was kindly provided by Stefan Pöhlmann (Deutsches Primatenzentrum GmbH, Germany). To generate the *myc*- and His-tagged version of the protein, GP sequence was subcloned to a pcDNA™3.1/*myc*-His(-) plasmid. The plasmid expressing Zaire ebolavirus matrix protein VP40 fused in-frame with the green fluorescent protein (GFP) (pVP40-GFP) was a gift from Christopher Basler (Mount Sinai School of Medicine, New York,

USA). The plasmid expressing the Vesicular Stomatitis Virus (VSV) glycoprotein (pVSV-G) was previously described [56]. The recombinant VSV encoding the luciferase in place of the VSV-G gene (VSVΔG-Luc) was provided by Michael Whitt, University of Tennessee, USA.

EBOV infection

HEK293 wild type and KO cells (WT, *C1GALT1C1* KO, *GALNT1* KO, *GALNT2* KO, and *GALNT3* KO) were seeded in T25 culture flasks in DMEM containing 10 % FBS and 50 U/mL penicillin/streptomycin (Thermo Fisher Scientific Cat. Nr. 15070). Twenty-four hours post-seeding, cells were infected with ZEBOV at an MOI of 0.1 in infection medium (DMEM containing 2 % FBS). One hour post-infection, input virus were discarded and cells were washed once with infection medium, added fresh complete medium and incubated further at 37 °C, 5 % CO_2. At one and six days post-infection, virus particles in the culture supernatant (progeny viruses) were harvested and clarified from cell debris by centrifugation at 1,500 rpm for 10 min. Titration of progeny viruses from all HEK293 cells was done in Vero-E6 cells cultured in 16-well chambered slides (Thermo Fisher Scientific), as described below. For RNA extraction, cells and cell culture supernatants were harvested in TRIzol reagent (Thermo Fisher Scientific) at day one and six post-infection. For immunofluorescence experiments, HEK293 wild type and knockout cells were grown on 12-well chambered glass slides and infected with ZEBOV at an MOI of 0.01 in DMEM containing 2 % FBS for 1 h at 37°C, 5 % CO_2. Thereafter input virus was discarded and new complete medium was added to each well and incubated further at 37 °C, 5 % CO_2. At 24 hours post-infection the slides were inactivated in acetone twice, first for 10 min and then transferring to another jar with new acetone and incubating for 30 min at room temperature.

Fluorescent focus forming assay

Infectivity of progeny viruses produced from HEK293 wild type and knockout cells were determined using infectious focus forming assay. Briefly, Vero-E6 cells cultured in 16-well chambered slides were infected with ten-fold serially diluted virus for 1 h at 37 °C, 5 % CO_2. Input virus were then discarded and fresh complete medium was added to the cells. At 24 hours post-infection, cells were fixed in acetone for 20 min. Cells were permeabilized in PBS that contained 0.1 % Triton X-100 for 5 min. Slides were then incubated with rabbit anti-EBOV GP primary

antibody (produced by Agrisera upon request) that was diluted in 150 mM NaCl for 1 h, washed three times in PBS and further incubated with FITC-conjugated goat anti-rabbit IgG (Thermo Fisher Scientific) as a secondary antibody for 30 min. All incubations were carried out at 37 °C. DAPI (4',6-diamidino-2-phenylindole dihydrochloride) was used to stain cell nuclei.

RT-qPCR

Samples from infected cells and cell culture supernatants were extracted using TRIzol reagent (Thermo Fisher Scientific). At day one and six post-infection, cell culture supernatants were harvested by mixing with TRIzol LS reagent (Thermo Fisher Scientific) at a ratio of 1 to 3. Cells in T25 culture flask were harvested in 1 mL TRIzol reagent. Prior to RNA extraction, TRIzol inactivated cells and cell culture supernatants were subjected to chloroform treatment, followed by RNA extraction using PSS magLEAD 12gC machine (Precision System Science Co.) and eluted the RNA with 100 µL elution buffer. Purified samples were stored at -80°C, pending analysis.
The ZEBOV RT-PCR assay was performed in a 25 µL reaction mixture containing TaqMan Fast Virus 1-step master mix (Thermo Fisher Scientific), 5 µl template RNA, 900 µM of each primer and 200 µM of TaqMan probe. The forward primer 5'- ATGGGCTGAAAAYTGCTACAATC and reverse primer 5'- CTTTGTGMACATASCGGCAC as well the probe FAM- CTACCAGCAGCGCCAGACGGGA-TAMRA were for amplification of ZEBOV GP gene. Amplification and detection of the vRNA was performed in a StepOne Plus real-time PCR machine (Applied Biosystems). The cycling conditions were as following: 50 °C for 5 min; 45 cycles of 95 °C for 20 sec and 95 °C for 3 sec and 60 °C for 30 sec. Human beta-actin was used as an endogenous gene control to confirm the integrity of the extraction reagent and RNA recovery as well as to normalize the levels of intracellular viral RNAs.

Ebola virus-like particle production

Zaire ebolavirus-Like particles (EBOVLPs) were produced by transfection of HEK293T cells with a plasmid expressing the EBOV matrix protein VP40 fused to GFP (VP40-GFP) along with a construct expressing either the ZEBOV GP – strain Makona, or the VSV envelope G glycoprotein. Cells seeded in 100 mm plates were transfected with 11.5 µg of pVP40-GFP and along with 0.5 µg of pcDNA3.1-ZEBOV-GP or pVSV-G by calcium-phosphate [57]. Cell culture supernatants were collected 48 hours after transfection, cell debris were cleared by centrifugation (1,200 rpm for 7 minutes at 4

°C). EBOVLPs production was confirmed by cytofluorimetric analyses of transduced Vero CCL81 cells as previously described [58]. Next, VLPs were purified and concentrated by two ultracentrifugation steps at 27,000 rpm for 2 hours in 20 % sucrose cushion, then aliquoted and stored at -80 °C.

Pseudotyped virus production and titration

ZEBOV GP pseudotyped VSVΔG-Luc (GP-pseudotyped virus) was generated as previously described [59]. Briefly, HEK293T cells were transfected by calcium-phosphate protocol with 16 µg of pcDNA3.1-ZEBOV-GP plasmid and, 24 h later, infected with the recombinant VSVΔG-Luc virus at the multiplicity of infection (MOI) of 4 fluorescent focus-forming units (FFU)/cell. After 24 h, the pseudotyped virus was harvested and stored at −80°C. Viral titer was evaluated as FFU/mL using the anti-VSV-Matrix protein 23H12 antibody (Kerafast Inc.) to detect infected cells.

EBOV-Pseudotype (pEBOV_KO) Production on HEK293 knockout cell lines

HEK293 were seeded in poly-Lysine-coated 6-well plates and transfected with the pcDNA3.1-ZEBOV-GP plasmid as above described. Six h later, cells were washed and fresh medium added. The day after, cells were infected for 1 h with the VSVΔG-Luc virus at MOI 4 FFU/cell, washed twice in PBS and incubated in complete medium for 14 h. Next, medium was recovered and centrifuged at 3,500 rpm at 4° C for 6 minutes to remove cellular debris. Then, aliquots were made and stored at -80° C for further use. The viral progeny production was evaluated infecting semi-confluent Vero-CCL-81 cells seeded in 96 well plates. After 1 h cells were washed in PBS and cultured for additional 24 h before the evaluation of the Luc expression using the Steady-Glo® Luciferase reagent (Promega), which were added to the cell for 15 minutes. The luminescence was detected with a VICTOR Multilabel Plate Reader (PerkinElmer) as relative-luminescence unit (RLU, normalized on a scale factor of 1 second).

pEBOV infection on HEK293 knockout lines

One day before the assay, $2x10^4$ HEK293 knockout cells were seeded in poly-Lysine-coated 96-well plates. The day after, cells were washed with PBS and infected with pEBOV at MOI 0.01 for 1 hour.

Then, cells were washed with PBS and new complete medium was added. After 24 h the reporter gene expression was detected, as above described, to evaluate the efficiency of infection.

Transfection

For immunofluorescence experiments the panel of HEK293 cells grown on poly-Lysine (Sigma-Aldrich Cat. Nr. P6282) pre-coated (2.5 μg/mL in MQ H_2O 30 min at room temperature (RT)) glass cover slips in 24-wells were transfected with 0.5 μg/well of pcDNA™3.1/*myc*-His(-) plasmid encoding *myc*- and His-tagged full-length EBOV GP (Zaire ebolavirus isolate Ebola virus/H.sapiens-wt/SLE/2014/Makona-G3838) using Lipofectamine™ 3000 (Thermo Fisher Scientific Cat. Nr. L3000) according to manufacturer's instructions. Non-transfected cells were used as controls. At 48 hours post-transfection the cells were washed 3x with Hanks' Balanced Salt solution (HBSS, Sigma-Aldrich Cat. Nr. H8264) and fixed with 4 % PFA in PBS (Ampliqon Cat. Nr. AMPQ44154.1000) for 10 min at RT followed by 3x more washes. If needed, the cells were permeabilized with 0.3 % Triton X-100 in HBSS for 3 min followed by 3x washes with PBS and blocked with 2.5 % BSA in PBS, 0.03 % sodium azide at 4 °C until staining. For Western blotting experiments the panel of HEK293 cells grown in 6-wells were transfected with 2 μg/well of the plasmid and harvested at 48 hours post-transfection. The cells were washed with PBS and lysed in modified RIPA buffer (50 mM Tris pH 7.5, 150 mM NaCl, 1 % NP-40, 0.1 % Na deoxycholate, 1 mM EDTA) supplemented with protease inhibitor cocktail (cOmplete™, EDTA-free, Roche Cat. Nr. 11873580001) and phosphatase inhibitors for 30 min at 4 °C with agitation, followed by sonication using a sonic probe on ice. The lysates were centrifuged at 10000 x g for 10 min at 4 °C and the supernatants used for subsequent Western blotting. For protein purification HEK293 WT, *GALNT1* KO, *GALNT2* KO, and *GALNT3* KO cells were grown in 3x P150 dishes each and transfected with 23 μg/dish of the plasmid and harvested at 48 hours post-transfection. The plates were chilled on ice, washed with ice-cold PBS twice and cells gently scraped in ice-cold PBS followed by centrifugation at 500 x g for 10 min at 4 °C. After decanting most of PBS, pellets were dislodged and pooled for each cell type, followed by centrifugation at 800 x g for 10 min at 4 °C. PBS was removed, and pellets stored at -80 °C.

EBOV GP purification

Cell pellets were thawed on ice in 0.1 % RapiGest (Waters Cat. Nr. 186001861) in Equilibration buffer (25 mM Tris-HCl 300 mM NaCl pH 7.5) supplemented with protease inhibitor cocktail (cOmplete™, EDTA-free, Roche Cat. Nr. 11873580001) followed by sonication using a sonic probe on ice. His-tagged proteins were purified using HisPur™ Ni-NTA resin (Thermo Fisher Scientific Cat. Nr. 88222) according to manufacturer's instructions (batch protocol). Briefly, the lysates were cleared by centrifugation at 10000 x g for 10 min at 4 °C and applied to pre-equillibrated HisPur™ Ni-NTA resin followed by a 1-hour incubation on an end-over-end rotator. The resin was washed 3x 5 min with Wash buffer (25 mM Tris-HCl 300 mM NaCl pH 7.5, 10 mM imidazole), and bound proteins eluted in Elution buffer (25 mM Tris-HCl 300 mM NaCl pH 7.5, 250 mM imidazole). Protein concentration was measured using Pierce™ 660 nm Protein Assay Kit (Thermo Fisher Scientific Cat. Nr. 22662) and 400 μg of each cell type-derived protein taken for subsequent MS sample preparation.

Immunofluorescence

Fixed cover slips or teflon-coated slides were incubated with primary antibodies diluted in 2.5 % BSA (Sigma-Aldrich Cat. Nr. A3294) in PBS, 0.03 % sodium azide over night at 4 °C: rabbit anti-EBOV GP (1:300, produced by Agrisera upon request), goat anti-E-cadherin (1:200, R&D Systems Cat. Nr. AF648), rabbit anti-Myc (1:200 Abcam Cat. Nr. ab152146) or undiluted hybridoma supernatants (mouse anti-GalNAc-T1 (4D8), mouse anti-GalNAc-T2 (4C4), mouse anti-GalNAc-T3 (2D10)), followed by 3x washes with PBS and 1-hour incubation at RT with secondary antibodies: donkey anti-rabbit IgG AF546 (1:500), donkey anti-goat IgG AF488 (1:500), goat anti-rabbit IgG AF488 (1:500), goat anti-mouse IgG AF594 (1:500), all from Thermo Fisher Scientific. After 3x washes with PBS cover slips were incubated with 0.1 μg/mL DAPI solution for 4 min followed by 3x washing and mounting with Prolong Gold antifade-reagent (Thermo Fisher Scientific Cat. Nr. P36930). Teflon-coated slides were mounted using Prolong Gold antifade-reagent with DAPI (Thermo Fisher Scientific Cat. Nr. P36935). Fluorescence micrographs and z-stacks were obtained on a Zeiss LSM710 confocal microscope. Images were assembled using Adobe Photoshop, Adobe Illustrator or Zeiss ZEN Lite software.

Western Blotting

30 μg of protein extracts were divided into two aliquots, one of which was treated with 2 U of PNGase F (Roche Cat. Nr. 11365177001) at 37 °C for 1 hour. Samples were then mixed with 4x NuPAGE sample buffer (Thermo Fisher Scientific Cat. Nr. B007) and 10 mM DTT, heat denatured (95 °C 5 min), and separated on Novex 4-12 % gradient gel (Bis-Tris) (Thermo Fisher Scientific Cat. Nr. NP0329) in 1x NuPAGE MES running buffer (Thermo Fisher Scientific Cat. Nr. NP0002), followed by transfer onto nitrocellulose membrane in 20 % MeOH in running buffer at 320 mA for 1 hour. Membranes were blocked with 5 % skim milk in TBS-T and blotted with rabbit anti-EBOV GP (1:800, produced by Agrisera upon request) antibody over night at 4 °C, followed by goat anti-rabbit Igs-HRP (1:4000, DAKO Cat. Nr. P0448) for 1 hour at RT. Membranes were developed using Pierce™ ECL Kit (Thermo Scientific) and visualized using the ImageQuant LAS4000 system.

Transmission electron microscopy

Cell culture supernatants from HEK293 WT and different KO cell lines harvested at 24 hours post-infection were inactivated by mixing 1:1 with 2.5 % freshly prepared glutaraldehyde and incubating for 1 h at room temperature. Samples were applied to copper grids (Gilder Grids, G400) and negative stained with phosphotungstic acid. Grids were analyzed using a CM100 transmission electron microscope (FEI/Philips) equipped with TWIN objective lens and a side-mounted Olympus Veleta camera with a resolution of 2048 x 2048 pixels (2K x 2K). Images were recorded using ITEM software.

O-glycoproteomic sample preparation

For differential O-glycoproteomic analysis, 400 μg of each cell type-derived protein in equal volumes of Elution buffer were diluted to 1 mL using 0.5 % RapiGest in 250 mM AmBic (ammonium hydrocarbonate) and H_2O resulting in a final concentration of 0.1 % RapiGest and 50 mM AmBic. Proteins were reduced by adding up to 5 mM dithiothreitol (DTT, Sigma-Aldrich Cat. Nr. D0632) and incubating at 60 °C for 45 min followed by alkylation with 10 mM iodoacetamide (IAA, Sigma-Aldrich Cat. Nr. I1149) at RT for 30 min in darkness. The proteins were then treated with 8 U PNGase F (Roche Cat. Nr. 11365177001) at 37 °C for 3 hours followed by 19 μg/sample of trypsin (Roche Cat. Nr. 11418025001) at 37 °C for 13 hours. Digests were acidified with trifluoracetic acid and peptides purified using Sep-Pak (1cc) C18 cartridges (Waters Cat. Nr.

WAT023590) (1x CV MeOH; 1x CV 50 % MeOH 0.1 % FA; 3x CV 0.1 % TFA; load twice; 3x CV 0.1 % FA; elute in 2x CV of 50 % MeOH 0.1 % FA (CV = column volume)). Peptide concentrations were measured using NanoDrop A205. 200 μg of peptides from each sample was taken, most of solvent evaporated using SpeedVac then added up to 1 mL H_2O and freeze dried. Dried peptides were reconstituted in 100 μL TEAB and labeled with TMTsixplex™ reagents (TMT 127, TMT 128, TMT 129, TMT 130, Thermo Fisher Scientific Cat. Nr. 90061) according to manufacturer's instructions. 1 % of each reaction was mixed, dried and submitted to LC-MS analysis for a ratio check. After confirming equal ratios all four channels were mixed and dried with SpeedVac. The peptide mix was then reconstituted in 50 mM sodium acetate pH 5 and treated with 0.25 U/mL *Clostridium perfringens* neuraminidase (Sigma-Aldrich Cat. Nr. N3001) at 37 °C for 3 hours. For O-glycoproteomic analysis of EBOV VLPs 300 μL of VLPs were diluted with 0.1 % RapiGest in 50 mM AmBic up to 1.3 mL, then sonicated using a sonic probe on ice, heated at 80 °C for 10 min and protein concentration measured using Pierce BCA™ Assay Kit. Approximately 800 μg of VLP lysate was then reduced and alkylated as described above and treated with 5 U PNGase F (Roche Cat. Nr. 11365177001) at 37 °C for 12 hours followed by 12 hours with 11 μg of trypsin. PNGase F treatment was then repeated followed by a 2-hour incubation with 4 μg of trypsin. Peptides were purified as described above, concentrated by SpeedVac and treated with 0.15 U/mL neuraminidase at 37 °C for 3 hours.

LWAC enrichment

Sequential PNA and VVA LWAC enrichment was performed as previously described [40]. Elution fractions were desalted using self-made Stage Tips (C18 sorbent from Empore 3M) and submitted to LC-MS and HCD/ETD-MS/MS.

Mass spectrometry analysis

LC MS/MS site-specific O-glycopeptide analysis of was performed on EASY-nLC1200 UHPLC (Thermo Fisher Scientific) interfaced via nanoSpray Flex ion source to an Orbitrap Fusion Lumos Tribrid MS (Thermo Fisher Scientific) or an on EASY-nLC1000 UHPLC (Thermo Fisher Scientific) interfaced via a PicoView nanoSpray ion source (New Objectives) to Orbitrap Fusion mass spectrometer (Thermo Fisher Scientific). The nLC was operated in a single analytical column set up

using PicoFrit Emitters (New Objectives, 75 mm inner diameter) packed in-house with Reprosil-Pure-AQ C18 phase (Dr. Maisch, 1.9-mm particle size, 19-21 cm column length). Each sample was injected onto the column and eluted in gradients from 3 to 32 % B in 95 min, from 32 to 100 % B in 10 min and 100 % B in 15 min at 200 nL/min (Solvent A, 100 % H_2O; Solvent B, 80 % acetonitrile; both containing 0.1 % (v/v) formic acid, EASY nLC-1200) and from 3 to 25 % B in 95 min, from 25 to 80 % B in 10 min and 80 % B in 15 min at 200 nL/min (Solvent A, 100 % H_2O; Solvent B, 100 % acetonitrile; both containing 0.1 % (v/v) formic acid, EASY nLC-1000).

A precursor MS1 scan (m/z 350–1,700) was acquired in the Orbitrap at the nominal resolution setting of 120,000, followed by Orbitrap HCD-MS2 and ETD-MS2 at the nominal resolution setting of 50,000 of the five most abundant multiply charged precursors in the MS1 spectrum; a minimum MS1 signal threshold of 50,000 was used for triggering data-dependent fragmentation events. For EBOVLP samples, stepped collision energy +/-5 % at 27 % was used for HCD MS/MS fragmentation and charge dependent calibrated ETD reaction time was used with CID supplemental activation at 30 % collision energy for ETD MS/MS fragmentation. For TMT-labelled samples, stepped collision energy +/-5 % at 45 % was used for HCD MS/MS fragmentation and charge dependent calibrated ETD reaction time was used with CID supplemental activation at 30 % collision energy for ETD MS/MS fragmentation.

For the site-specific glycopeptide identification, the corresponding HCD MS/MS and ETD MS/MS data were analyzed by Proteome discoverer 1.4 Software (Thermo Fisher Scientific) for EBOVLP samples or Proteome discoverer 2.2 software (Thermo Fisher Scientific) for EBOV GP samples using Sequest HT as a searching engine. Carbamidomethylation at cysteine was used as fixed modification and oxidation at methionine, asparagine deamidation, and HexNAc, Hex1HexNAc1, Hex1HexNAc2, and Hex2HexNAc2 at serine/threonine/tyrosine were used as variable modifications. Precursor mass tolerance was set to 10 ppm and fragment ion mass tolerance was set to 0.02 Da. Data were searched against the human-specific UniProt KB/SwissProt-reviewed database downloaded on January, 2013 and construct-dependent viral protein sequence databases. All spectra of interest were manually inspected and validated to prove the correct peptide identification and glycosite localization.

References

1. Bornholdt ZA, Turner HL, Murin CD, Li W, Sok D, Souders CA, Piper AE, Goff A, Shamblin JD, Wollen SE*, et al.* (2016) Isolation of potent neutralizing antibodies from a survivor of the 2014 Ebola virus outbreak. *Science* **351**: 1078-83
2. Gilchuk P, Murin CD, Milligan JC, Cross RW, Mire CE, Ilinykh PA, Huang K, Kuzmina N, Altman PX, Hui S*, et al.* (2020) Analysis of a Therapeutic Antibody Cocktail Reveals Determinants for Cooperative and Broad Ebolavirus Neutralization. *Immunity* **52**: 388-403.e12
3. Audet J, Wong G, Wang H, Lu G, Gao GF, Kobinger G, Qiu X (2014) Molecular characterization of the monoclonal antibodies composing ZMAb: a protective cocktail against Ebola virus. *Sci Rep* **4**: 6881
4. Matz KM, Marzi A, Feldmann H (2019) Ebola vaccine trials: progress in vaccine safety and immunogenicity. *Expert Rev Vaccines* **18**: 1229-1242
5. Regules JA, Beigel JH, Paolino KM, Voell J, Castellano AR, Hu Z, Muñoz P, Moon JE, Ruck RC, Bennett JW*, et al.* (2017) A Recombinant Vesicular Stomatitis Virus Ebola Vaccine. *N Engl J Med* **376**: 330-341
6. Volchkov VE, Feldmann H, Volchkova VA, Klenk HD (1998) Processing of the Ebola virus glycoprotein by the proprotein convertase furin. *Proc Natl Acad Sci U S A* **95**: 5762-7
7. Gong X, Qian H, Zhou X, Wu J, Wan T, Cao P, Huang W, Zhao X, Wang X, Wang P*, et al.* (2016) Structural Insights into the Niemann-Pick C1 (NPC1)-Mediated Cholesterol Transfer and Ebola Infection. *Cell* **165**: 1467-1478
8. Lee J, Nyenhuis DA, Nelson EA, Cafiso DS, White JM, Tamm LK (2017) Structure of the Ebola virus envelope protein MPER/TM domain and its interaction with the fusion loop explains their fusion activity. *Proc Natl Acad Sci U S A* **114**: E7987-e7996
9. Nanbo A, Imai M, Watanabe S, Noda T, Takahashi K, Neumann G, Halfmann P, Kawaoka Y (2010) Ebolavirus is internalized into host cells via macropinocytosis in a viral glycoprotein-dependent manner. *PLoS Pathog* **6**: e1001121
10. Wang H, Shi Y, Song J, Qi J, Lu G, Yan J, Gao GF (2016) Ebola Viral Glycoprotein Bound to Its Endosomal Receptor Niemann-Pick C1. *Cell* **164**: 258-268
11. Zhang Q, Yang J, Tillieux S, Guo Z, Natividade RDS, Koehler M, Petitjean S, Cui Z, Alsteens D (2022) Stepwise Enzymatic-Dependent Mechanism of Ebola Virus Binding to Cell Surface Receptors Monitored by AFM. *Nano Lett*
12. Hood CL, Abraham J, Boyington JC, Leung K, Kwong PD, Nabel GJ (2010) Biochemical and structural characterization of cathepsin L-processed Ebola virus glycoprotein: implications for viral entry and immunogenicity. *J Virol* **84**: 2972-82
13. Kaletsky RL, Simmons G, Bates P (2007) Proteolysis of the Ebola virus glycoproteins enhances virus binding and infectivity. *J Virol* **81**: 13378-84
14. Bale S, Liu T, Li S, Wang Y, Abelson D, Fusco M, Woods VL, Jr., Saphire EO (2011) Ebola virus glycoprotein needs an additional trigger, beyond proteolytic priming for membrane fusion. *PLoS Negl Trop Dis* **5**: e1395
15. Chandran K, Sullivan NJ, Felbor U, Whelan SP, Cunningham JM (2005) Endosomal proteolysis of the Ebola virus glycoprotein is necessary for infection. *Science* **308**: 1643-5
16. Bagdonaite I, Wandall HH (2018) Global aspects of viral glycosylation. *Glycobiology* **28**: 443-467
17. Schjoldager KT, Narimatsu Y, Joshi HJ, Clausen H (2020) Global view of human protein glycosylation pathways and functions. *Nat Rev Mol Cell Biol* **21**: 729-749

18. Bagdonaite I, Vakhrushev SY, Joshi HJ, Wandall HH (2018) Viral glycoproteomes: technologies for characterization and outlook for vaccine design. *FEBS Lett* **592**: 3898-3920
19. Shajahan A, Supekar NT, Gleinich AS, Azadi P (2020) Deducing the N- and O-glycosylation profile of the spike protein of novel coronavirus SARS-CoV-2. *Glycobiology* **30**: 981-988
20. Watanabe Y, Allen JD, Wrapp D, McLellan JS, Crispin M (2020) Site-specific glycan analysis of the SARS-CoV-2 spike. *Science* **369**: 330-333
21. Zhao P, Praissman JL, Grant OC, Cai Y, Xiao T, Rosenbalm KE, Aoki K, Kellman BP, Bridger R, Barouch DH*, et al.* (2020) Virus-Receptor Interactions of Glycosylated SARS-CoV-2 Spike and Human ACE2 Receptor. *Cell Host Microbe* **28**: 586-601.e6
22. Bennett EP, Mandel U, Clausen H, Gerken TA, Fritz TA, Tabak LA (2012) Control of mucin-type O-glycosylation: a classification of the polypeptide GalNAc-transferase gene family. *Glycobiology* **22**: 736-56
23. Bagdonaite I, Pallesen EM, Ye Z, Vakhrushev SY, Marinova IN, Nielsen MI, Kramer SH, Pedersen SF, Joshi HJ, Bennett EP*, et al.* (2020) O-glycan initiation directs distinct biological pathways and controls epithelial differentiation. *EMBO Rep* **21**: e48885
24. Schjoldager KT, Vakhrushev SY, Kong Y, Steentoft C, Nudelman AS, Pedersen NB, Wandall HH, Mandel U, Bennett EP, Levery SB*, et al.* (2012) Probing isoform-specific functions of polypeptide GalNAc-transferases using zinc finger nuclease glycoengineered SimpleCells. *Proceedings of the National Academy of Sciences of the United States of America* **109**: 9893-8
25. Lavrsen K, Dabelsteen S, Vakhrushev SY, Levann AMR, Haue AD, Dylander A, Mandel U, Hansen L, Frodin M, Bennett EP*, et al.* (2018) De novo expression of human polypeptide N-acetylgalactosaminyltransferase 6 (GalNAc-T6) in colon adenocarcinoma inhibits the differentiation of colonic epithelium. *The Journal of biological chemistry* **293**: 1298-1314
26. Narimatsu Y, Joshi H, Schjoldager KT, Hintze J, Halim A, Steentoft C, Nasson R, Mandel U, Bennett EP, Clausen H*, et al.* (2019) Exploring Regulation of Protein O-Glycosylation in Isogenic Human HEK293 Cells by Differential O-Glycoproteomics. *Molecular & cellular proteomics : MCP*
27. Wandall HH, Nielsen MAI, King-Smith S, de Haan N, Bagdonaite I (2021) Global functions of O-glycosylation: promises and challenges in O-glycobiology. *Febs j*
28. de Haan N, Narimatsu Y, Koed Møller Aasted M, Larsen ISB, Marinova IN, Dabelsteen S, Vakhrushev SY, Wandall HH (2022) In-Depth Profiling of O-Glycan Isomers in Human Cells Using C18 Nanoliquid Chromatography-Mass Spectrometry and Glycogenomics. *Anal Chem* **94**: 4343-4351
29. Iraqi M, Edri A, Greenshpan Y, Kundu K, Bolel P, Cahana A, Ottolenghi A, Gazit R, Lobel L, Braiman A*, et al.* (2020) N-Glycans Mediate the Ebola Virus-GP1 Shielding of Ligands to Immune Receptors and Immune Evasion. *Front Cell Infect Microbiol* **10**: 48
30. Dowling W, Thompson E, Badger C, Mellquist JL, Garrison AR, Smith JM, Paragas J, Hogan RJ, Schmaljohn C (2007) Influences of glycosylation on antigenicity, immunogenicity, and protective efficacy of ebola virus GP DNA vaccines. *J Virol* **81**: 1821-37
31. Feldmann H, Nichol ST, Klenk HD, Peters CJ, Sanchez A (1994) Characterization of filoviruses based on differences in structure and antigenicity of the virion glycoprotein. *Virology* **199**: 469-73
32. Lee JE, Saphire EO (2009) Ebolavirus glycoprotein structure and mechanism of entry. *Future virology* **4**: 621-635

33. Fujihira H, Usami K, Matsuno K, Takeuchi H, Denda-Nagai K, Furukawa JI, Shinohara Y, Takada A, Kawaoka Y, Irimura T (2018) A Critical Domain of Ebolavirus Envelope Glycoprotein Determines Glycoform and Infectivity. *Sci Rep* **8**: 5495
34. Rutten L, Gilman MSA, Blokland S, Juraszek J, McLellan JS, Langedijk JPM (2020) Structure-Based Design of Prefusion-Stabilized Filovirus Glycoprotein Trimers. *Cell Rep* **30**: 4540-4550.e3
35. Yang ZY, Duckers HJ, Sullivan NJ, Sanchez A, Nabel EG, Nabel GJ (2000) Identification of the Ebola virus glycoprotein as the main viral determinant of vascular cell cytotoxicity and injury. *Nat Med* **6**: 886-9
36. Luczkowiak J, Lasala F, Mora-Rillo M, Arribas JR, Delgado R (2018) Broad Neutralizing Activity Against Ebolaviruses Lacking the Mucin-Like Domain in Convalescent Plasma Specimens From Patients With Ebola Virus Disease. *J Infect Dis* **218**: S574-s581
37. Hintze J, Ye Z, Narimatsu Y, Madsen TD, Joshi HJ, Goth CK, Linstedt A, Bachert C, Mandel U, Bennett EP*, et al.* (2018) Probing the contribution of individual polypeptide GalNAc-transferase isoforms to the O-glycoproteome by inducible expression in isogenic cell lines. *J Biol Chem* **293**: 19064-19077
38. Mao Y, Wang S, Zhao Y, Konstantinidi A, Sun L, Ye Z, Vakhrushev SY (2021) Systematic Evaluation of Fragmentation Methods for Unlabeled and Isobaric Mass Tag-Labeled O-Glycopeptides. *Anal Chem* **93**: 11167-11175
39. Simon EJ, Linstedt AD (2018) Site-specific glycosylation of Ebola virus glycoprotein by human polypeptide GalNAc-transferase 1 induces cell adhesion defects. *J Biol Chem* **293**: 19866-19873
40. Bagdonaite I, Norden R, Joshi HJ, Dabelsteen S, Nystrom K, Vakhrushev SY, Olofsson S, Wandall HH (2015) A strategy for O-glycoproteomics of enveloped viruses--the O-glycoproteome of herpes simplex virus type 1. *PLoS pathogens* **11**: e1004784
41. Spillings BL, Day CJ, Garcia-Minambres A, Aggarwal A, Condon ND, Haselhorst T, Purcell DFJ, Turville SG, Stow JL, Jennings MP*, et al.* (2022) Host glycocalyx captures HIV proximal to the cell surface via oligomannose-GlcNAc glycan-glycan interactions to support viral entry. *Cell reports* **38**: 110296
42. de Las Rivas M, Lira-Navarrete E, Gerken TA, Hurtado-Guerrero R (2019) Polypeptide GalNAc-Ts: from redundancy to specificity. *Curr Opin Struct Biol* **56**: 87-96
43. Bagdonaite I, Pallesen EMH, Nielsen MI, Bennett EP, Wandall HH (2021) Mucin-Type O-GalNAc Glycosylation in Health and Disease. *Adv Exp Med Biol* **1325**: 25-60
44. de Las Rivas M, Lira-Navarrete E, Daniel EJP, Compañón I, Coelho H, Diniz A, Jiménez-Barbero J, Peregrina JM, Clausen H, Corzana F*, et al.* (2017) The interdomain flexible linker of the polypeptide GalNAc transferases dictates their long-range glycosylation preferences. *Nat Commun* **8**: 1959
45. Fritz TA, Hurley JH, Trinh LB, Shiloach J, Tabak LA (2004) The beginnings of mucin biosynthesis: the crystal structure of UDP-GalNAc:polypeptide alpha-N-acetylgalactosaminyltransferase-T1. *Proc Natl Acad Sci U S A* **101**: 15307-12
46. Pedersen JW, Bennett EP, Schjoldager KT, Meldal M, Holmér AP, Blixt O, Cló E, Levery SB, Clausen H, Wandall HH (2011) Lectin domains of polypeptide GalNAc transferases exhibit glycopeptide binding specificity. *J Biol Chem* **286**: 32684-96
47. Brokx RD, Revers L, Zhang Q, Yang S, Mal TK, Ikura M, Gariépy J (2003) Nuclear magnetic resonance-based dissection of a glycosyltransferase specificity for the mucin MUC1 tandem repeat. *Biochemistry* **42**: 13817-25

48. Tetaert D, Ten Hagen KG, Richet C, Boersma A, Gagnon J, Degand P (2001) Glycopeptide N-acetylgalactosaminyltransferase specificities for O-glycosylated sites on MUC5AC mucin motif peptides. *Biochem J* **357**: 313-20
49. Wilson JA, Hevey M, Bakken R, Guest S, Bray M, Schmaljohn AL, Hart MK (2000) Epitopes involved in antibody-mediated protection from Ebola virus. *Science* **287**: 1664-6
50. Khurana S, Ravichandran S, Hahn M, Coyle EM, Stonier SW, Zak SE, Kindrachuk J, Davey RT, Jr., Dye JM, Chertow DS (2020) Longitudinal Human Antibody Repertoire against Complete Viral Proteome from Ebola Virus Survivor Reveals Protective Sites for Vaccine Design. *Cell Host Microbe* **27**: 262-276.e4
51. Sanchez-Lockhart M, Reyes DS, Gonzalez JC, Garcia KY, Villa EC, Pfeffer BP, Trefry JC, Kugelman JR, Pitt ML, Palacios GF (2018) Qualitative Profiling of the Humoral Immune Response Elicited by rVSV-ΔG-EBOV-GP Using a Systems Serology Assay, Domain Programmable Arrays. *Cell Rep* **24**: 1050-1059.e5
52. Heidepriem J, Krähling V, Dahlke C, Wolf T, Klein F, Addo MM, Becker S, Loeffler FF (2020) Epitopes of Naturally Acquired and Vaccine-induced Anti-Ebola Virus Glycoprotein Antibodies in Single Amino Acid Resolution. *Biotechnol J*: e2000069
53. Ponomarenko J, Vaughan K, Sette A, Maurer-Stroh S (2014) Conservancy of mAb Epitopes in Ebolavirus Glycoproteins of Previous and 2014 Outbreaks. *PLoS Curr* **6**
54. Narimatsu Y, Joshi HJ, Schjoldager KT, Hintze J, Halim A, Steentoft C, Nason R, Mandel U, Bennett EP, Clausen H*, et al.* (2019) Exploring Regulation of Protein O-Glycosylation in Isogenic Human HEK293 Cells by Differential O-Glycoproteomics. *Mol Cell Proteomics* **18**: 1396-1409
55. Steentoft C, Vakhrushev SY, Joshi HJ, Kong Y, Vester-Christensen MB, Schjoldager KT, Lavrsen K, Dabelsteen S, Pedersen NB, Marcos-Silva L*, et al.* (2013) Precision mapping of the human O-GalNAc glycoproteome through SimpleCell technology. *Embo j* **32**: 1478-88
56. Salata C, Curtarello M, Calistri A, Sartori E, Sette P, de Bernard M, Parolin C, Palù G (2009) vOX2 glycoprotein of human herpesvirus 8 modulates human primary macrophages activity. *J Cell Physiol* **219**: 698-706
57. Calistri A, Del Vecchio C, Salata C, Celestino M, Celegato M, Göttlinger H, Palù G, Parolin C (2009) Role of the feline immunodeficiency virus L-domain in the presence or absence of Gag processing: involvement of ubiquitin and Nedd4-2s ligase in viral egress. *J Cell Physiol* **218**: 175-82
58. Salata C, Munegato D, Martelli F, Parolin C, Calistri A, Baritussio A, Palù G (2018) Amiodarone affects Ebola virus binding and entry into target cells. *New Microbiol* **41**: 162-164
59. Salata C, Baritussio A, Munegato D, Calistri A, Ha HR, Bigler L, Fabris F, Parolin C, Palù G, Mirazimi A (2015) Amiodarone and metabolite MDEA inhibit Ebola virus infection by interfering with the viral entry process. *Pathog Dis* **73**

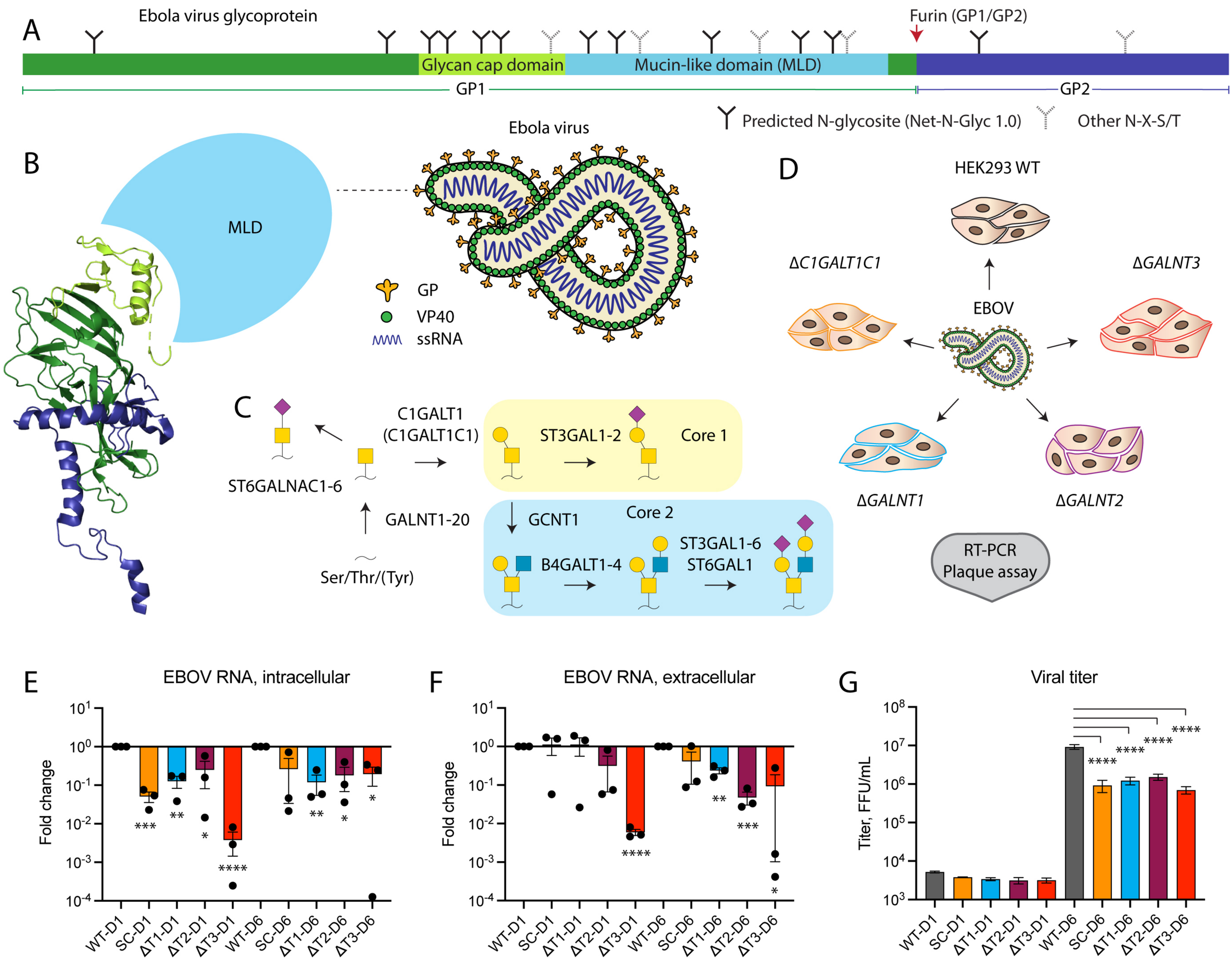

Figure 1. O-glycosylation is important for EBOV infectivity. (A) Layout of Ebola virus glycoprotein. (B) Cartoon depiction of Ebola virus, as well as a ribbon diagram of a monomeric viral envelope glycoprotein (PDB: 6VKM). Color coding as in (A). The mucin-like domain is not resolved and shown as a light blue sphere. (C) Predominant O-glycosylation pathways in HEK293 cells. (D) Experimental strategy for addressing the functional role of O-glycosylation in EBOV biology. (E, F) RT-PCR analysis of viral RNA day 1 (D1) and day 6 (D6) post-infection of glycoengineered HEK293 cells. Expression levels are normalized to β-actin, and presented as fold change compared to wild type. Data is shown as mean ±SEM of three independent experiments, where individual datapoints are also shown. One sample *t* test was used to evaluate differences from 1 (* $p < 0.05$, ** $p < 0.01$, *** $p < 0.001$, **** $p < 0.0001$). (E) Intracellular RNA. (F) Extracellular RNA. (G) Plaque titration analysis of Ebola virus in cell culture supernatants of infected glycoengineered cells on day 1 (D1) and day 6 (D6) post-infection. Data is shown as mean ±SEM of two independent experiments. One-way ANOVA followed by Šidák's multiple comparison test was used to evaluate differences in titers compared to wild type on the individual days post-infection (* $p < 0.05$, ** $p < 0.01$, *** $p < 0.001$, **** $p < 0.0001$).

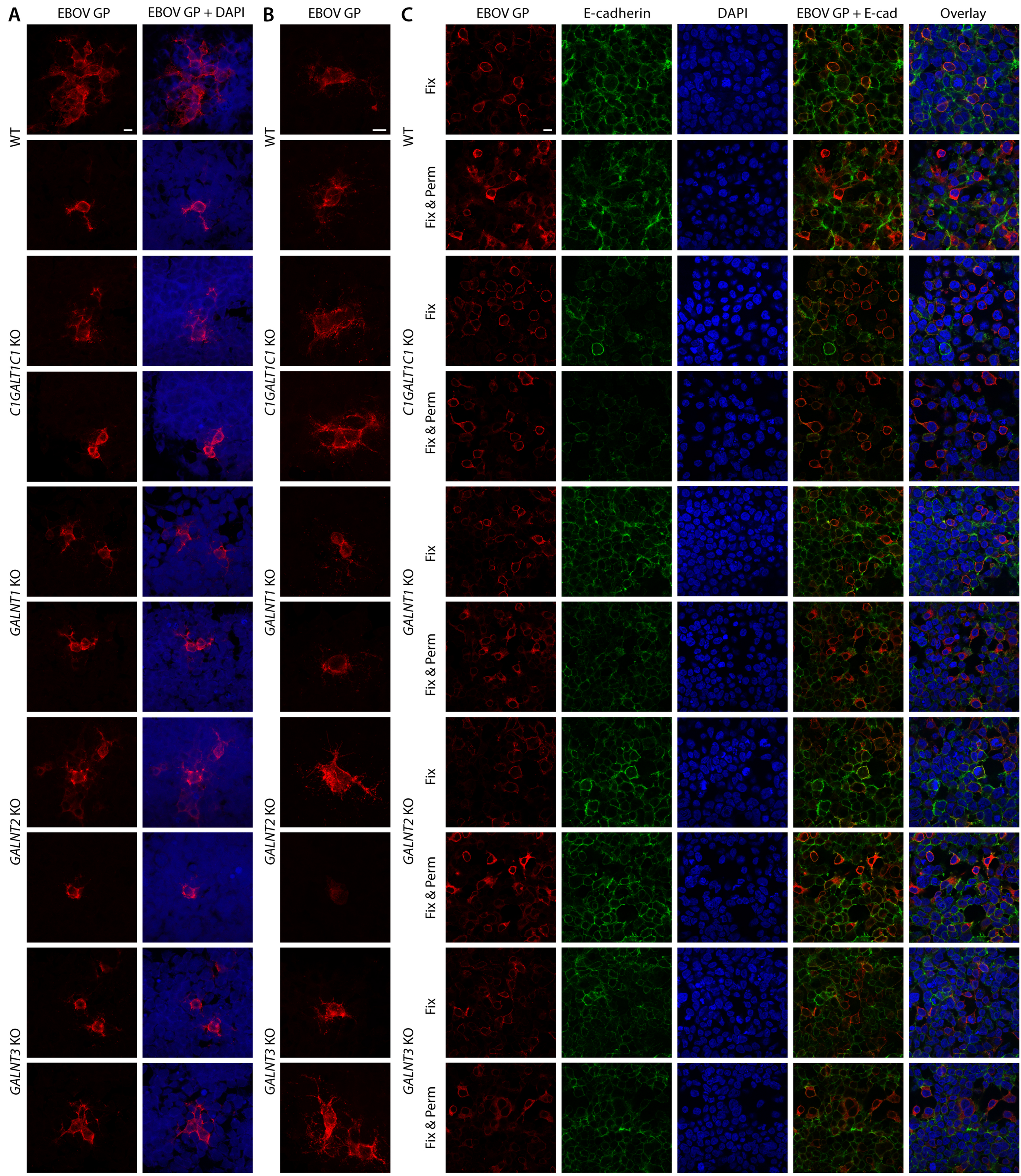

Figure 2. EBOV GP expression in glycoengineered cell lines. (A, B) Indicated HEK293 knock out cell lines grown on teflon-coted slides were infected with the Makona isolate of Zaire EBOV at 0.01 MOI, and fixed in acetone 24 hours post-infection. Cells were stained using rabbit α EBOV GP antibody (red). Two images for each cell line are shown. (A) Confocal snapshots. Scale bar 10 µm. (B) z-stack maximal intensity projections. Scale bar 10 µm. (C) Indicated cell lines grown on glass cover slips were transfected with a plasmid encoding full length EBOV Makona GP. 48 hours post-transfection cells were fixed with 4 % PFA (Fix) and co-stained for GP (red) and E-cadherin (green). Another set of cells was also permeabilized with 0.3 % Triton X-100 (Fix & Perm). Scale bar 10 µm.

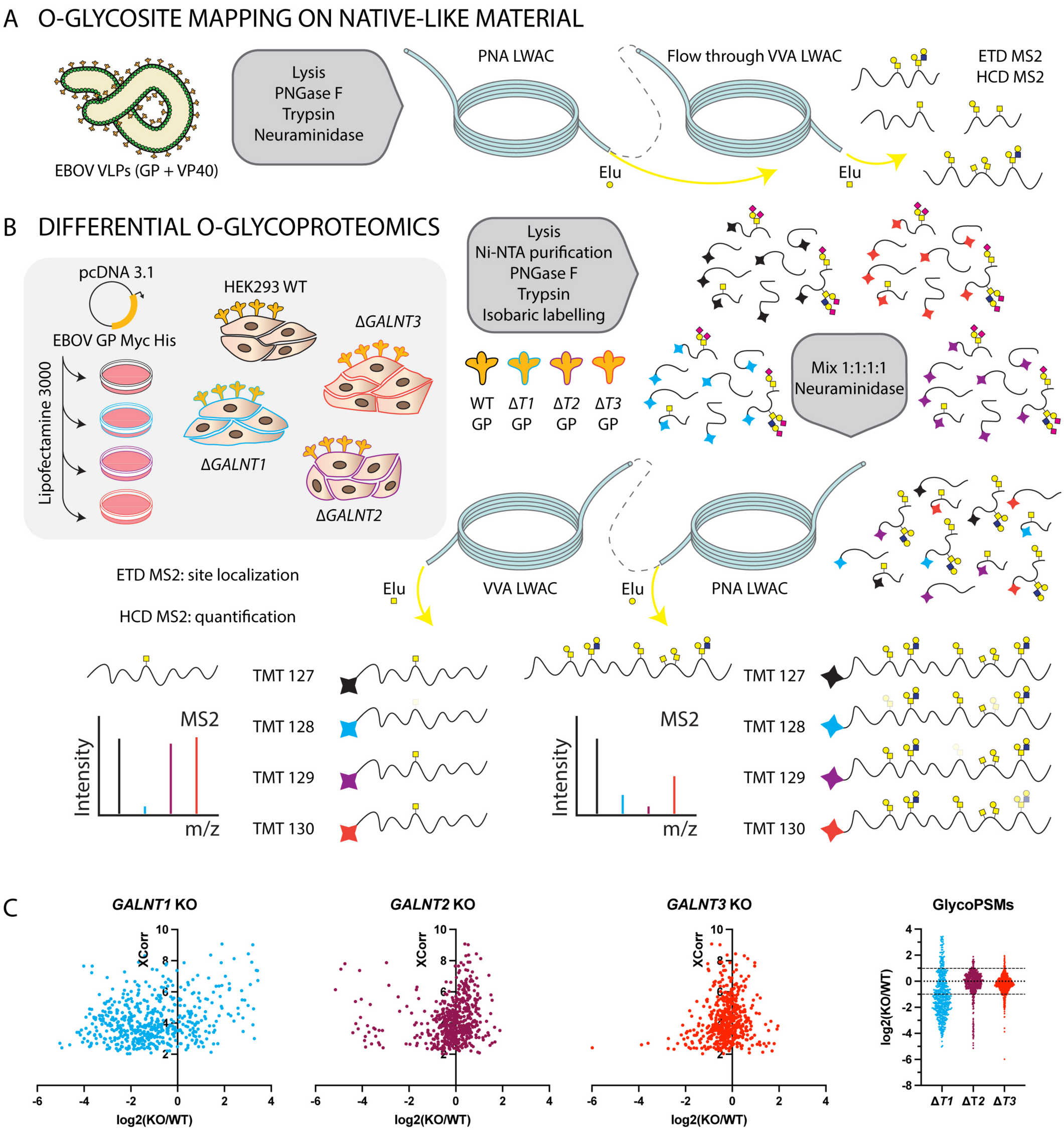

Figure 3. A strategy for Ebola virus O-glycoproteomics. (A) Approach for mapping O-glycosites on Ebola virus-like particles comprised of GP and VP40 proteins. (B) Approach for mapping differentially glycosylated O-glycosites on full-length reombinant GP expressed in *GALNT* KO cell lines. (C) The dot plots depict distribution of TMT quantification ratios compared to wild type (log_2) for glycopeptide PSMs (peptide spectrum matches) identified in both PNA and VVA LWAC experiments plotted against XCorr (cross-correlation score) values.

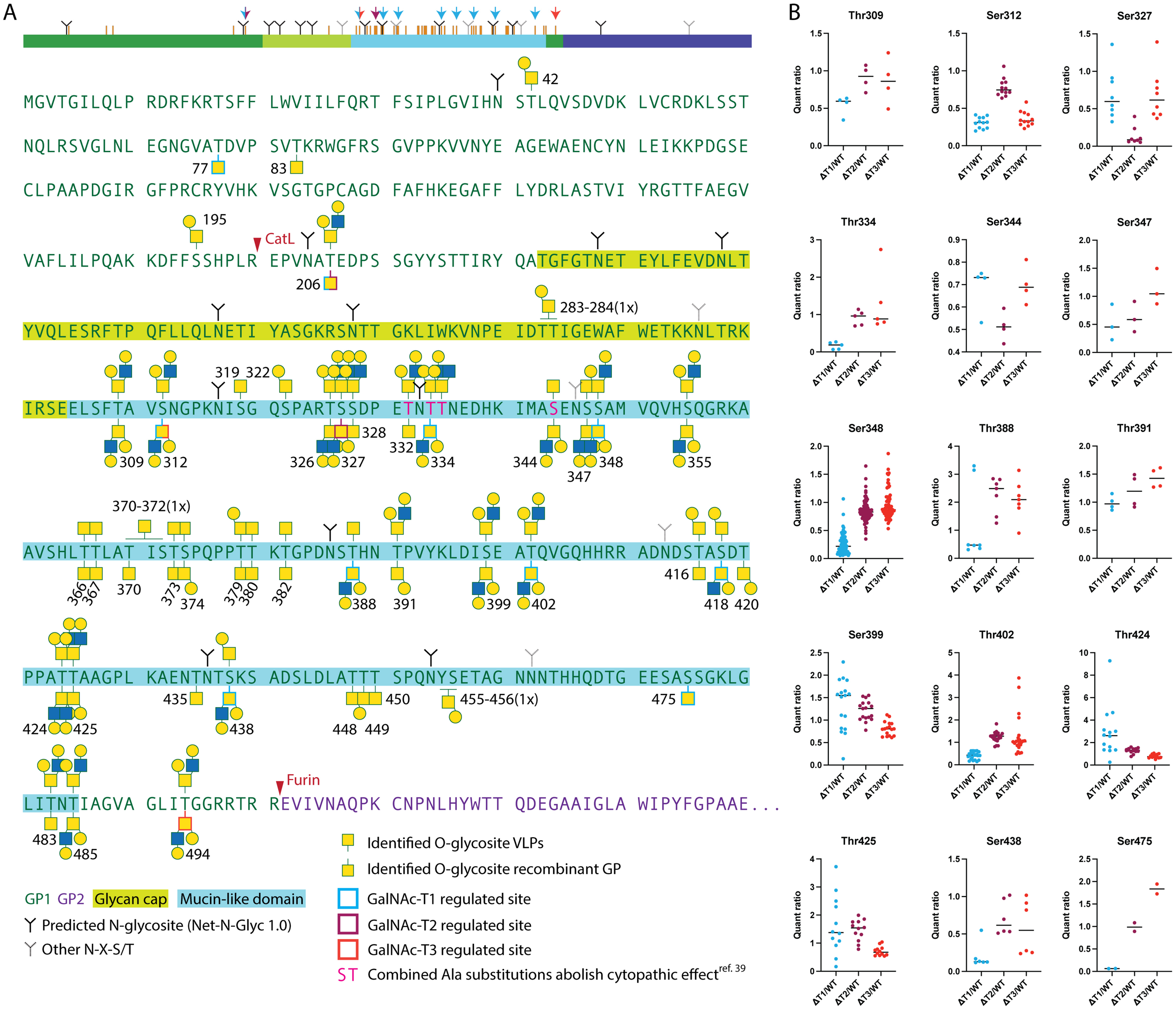

Figure 4. Mapping isoform-specific O-glycosites on EBOV GP. (A) Identified O-glycosites and most-complex unambiguously assigned site-specific structures are shown in the context of EBOV GP primary sequence, where VLP-derived sites are shown above the sequence, and recombinant GP-derived sites - below the sequence. Glycosites with median quantification ratios of singly glycosylated peptides below 0.5 were considered as isoform regulated and are outlined in cyan, maroon, and red for GalNAc-T1, GalNAc-T2, and GalNAc-T3, respectively. A simplified cartoon above summarizes the data, where orange bars represent all identified O-glycosites. Color coded arrows indicate isoform-regulated glycosites. (B) TMT quantification ratios of single site peptides, where each dot represents a separate PSM, and horizontal bars indicate median values.

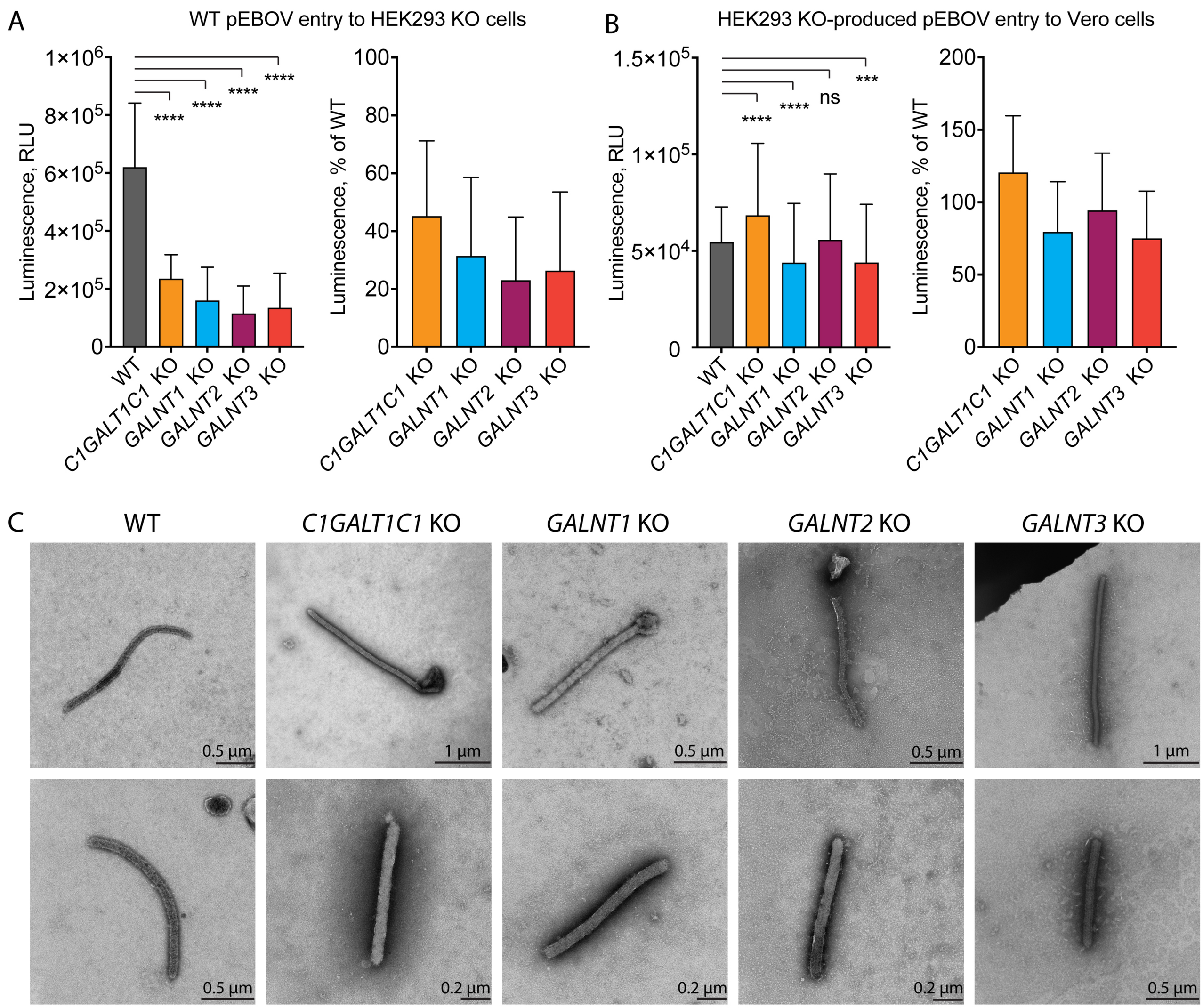

Figure 5. Influence of GalNAc-Ts on EBOV biology. (A) Entry of pEBOV-VSVΔGLuc to different HEK293 KO cells shown as reporter gene expression 24 hours post-infection. The data is shown as mean +SD of 5 biological replicates from 3 independent experiments. Two-way ANOVA followed by Dunnett's multiple comparison test was used to evaluate differences from wild type (* $p < 0.05$, ** $p < 0.01$, *** $p < 0.001$, **** $p < 0.0001$). (B) Titers of HEK293 KO cell line-produced pEBOV-VSVΔGLuc harvested 14 hours post-infection and assayed on Vero cells by measuring reporter gene expression 24 hours post-infection. The data is shown as mean +SD of 8 biological replicates from 4 independent experiments. Two-way ANOVA followed by Dunnett's multiple comparison test was used to evaluate differences from wild type (* $p < 0.05$, ** $p < 0.01$, *** $p < 0.001$, **** $p < 0.0001$). (C) TEM micrographs of Ebola virions produced in the panel of glycoengineered cell lines 24 hours post-infection. Negative staining with phosphotungstic acid was used for contrasting the specimens. Scale bar is indicated on each image.

Table 1. O-glycosites and structures

Glycosite	Recombinant GP PNA	Recombinant GP FT VVA	GalNAc-T regulation	Median KO/WT	VLPs PNA	VLPs FT VVA
Thr42					Hex1HexNAc1	HexNAc
Thr77		HexNAc	GalNAc-T1	0.43		
Thr83		HexNAc				
Ser195					Hex1HexNAc1	
Thr206		HexNAc	GalNAc-T1; GalNAc-T2	0.42; 0.27	Hex1HexNAc1, Hex2HexNAc2	HexNAc
283-284					Hex1HexNAc1	
Thr309	Hex1HexNAc1, Hex1HexNAc2, Hex2HexNAc2				Hex1HexNAc1, Hex2HexNAc2	HexNAc
Ser312	HexNAc, Hex1HexNAc1, Hex1HexNAc2, Hex2HexNAc2	HexNAc	GalNAc-T1; GalNAc-T3	0.31; 0.33	Hex1HexNAc1, Hex2HexNAc2	HexNAc
Ser319					HexNAc	
Ser322					HexNAc, Hex1HexNAc1	
Thr326	Hex1HexNAc1, Hex1HexNAc2, Hex2HexNAc2	HexNAc			HexNAc Hex1HexNAc1, Hex2HexNAc2	
Ser327	HexNAc, Hex1HexNAc1, Hex1HexNAc2, Hex2HexNAc2		GalNAc-T2	0.09	HexNAc, Hex1HexNAc1, Hex1HexNAc2, Hex2HexNAc2	HexNAc
Ser328		HexNAc			HexNAc, Hex1HexNAc1, Hex2HexNAc2	
Thr332		HexNAc			HexNAc, Hex1HexNAc1, Hex2HexNAc2	
Thr334	Hex1HexNAc1, Hex1HexNAc2, Hex2HexNAc2	HexNAc	GalNAc-T1	0.19	Hex2HexNAc2	
Thr335					Hex1HexNAc2	HexNAc
Ser344	HexNAc, Hex2HexNAc2				HexNAc, Hex1HexNAc1, Hex2HexNAc2	
Ser347	HexNAc, Hex1HexNAc1, Hex2HexNAc2				HexNAc, Hex2HexNAc2	
Ser348	HexNAc, Hex1HexNAc1, Hex1HexNAc2, Hex2HexNAc2	HexNAc, Hex1HexNAc1, Hex2HexNAc2	GalNAc-T1	0.22	HexNAc, Hex1HexNAc1, Hex2HexNAc2	HexNAc
Thr355	Hex2HexNAc2	HexNAc			HexNAc, Hex1HexNAc1, Hex2HexNAc2	
Thr366	HexNAc	HexNAc				HexNAc

Thr367	HexNAc	HexNAc			Hex1HexNAc1 (1x)	HexNAc
Thr370	HexNAc (2x)	HexNAc				HexNAc (1x)
Ser372					Hex1HexNAc1 (1x)	
Thr373		HexNAc				HexNAc
Ser374	Hex1HexNAc1	HexNAc				HexNAc
Thr379	HexNAc	HexNAc			Hex1HexNAc1	HexNAc
Thr380	HexNAc	HexNAc				HexNAc
Thr382		HexNAc				HexNAc
Thr388	Hex1HexNAc1, Hex2HexNAc2	HexNAc	GalNAc-T1	0.47	HexNAc	HexNAc
Thr391	Hex1HexNAc1	HexNAc			Hex1HexNAc1, Hex1HexNAc2, Hex2HexNAc2	HexNAc
Ser399	HexNAc, Hex1HexNAc1, Hex1HexNAc2, Hex2HexNAc2	HexNAc			HexNAc, Hex1HexNAc1, Hex1HexNAc2, Hex2HexNAc2	HexNAc
Thr402	HexNAc, Hex1HexNAc1, Hex1HexNAc2, Hex2HexNAc2	HexNAc	GalNAc-T1	0.43	HexNAc, Hex1HexNAc1, Hex1HexNAc2, Hex2HexNAc2	HexNAc
Thr416	HexNAc	HexNAc			HexNAc Hex1HexNAc1	HexNAc
Ser418	HexNAc, Hex1HexNAc2	HexNAc	GalNAc-T1	0.31	HexNAc, Hex1HexNAc1	
Thr420	Hex1HexNAc1	HexNAc				
Thr424	HexNAc, Hex1HexNAc1, Hex1HexNAc2, Hex2HexNAc2	HexNAc			Hex1HexNAc1, Hex2HexNAc2	HexNAc
Thr425	HexNAc, Hex1HexNAc1, Hex1HexNAc2, Hex2HexNAc2	HexNAc			HexNAc, Hex1HexNAc1, Hex2HexNAc2	HexNAc
Thr435		HexNAc				
Ser438	HexNAc, Hex1HexNAc1, Hex1HexNAc2, Hex2HexNAc2	HexNAc	GalNAc-T1	0.13	HexNAc, Hex1HexNAc1	HexNAc
Thr448	Hex1HexNAc1	HexNAc				
Thr449		HexNAc				
Thr450		HexNAc				
455-456 (1x)	Hex1HexNAc1					
Ser475		HexNAc	GalNAc-T1	0.06		
Thr483		HexNAc			Hex1HexNAc1, Hex2HexNAc2	
Thr485	Hex2HexNAc2	HexNAc			Hex1HexNAc1, Hex2HexNAc2	HexNAc

Thr494	Hex1HexNAc1, Hex2HexNAc2	HexNAc	GalNAc-T3	0.3	Hex1HexNAc1, Hex2HexNAc2	HexNAc